


PRIMARY RESEARCH

Open Access



PGM1 suppresses colorectal cancer cell migration and invasion by regulating the PI3K/AKT pathway

Zhewen Zheng^{1†}, Xue Zhang^{2†}, Jian Bai³, Long Long¹, Di Liu¹ and Yunfeng Zhou^{1*} 

Abstract

Background: Phosphoglucomutase 1 (PGM1) is known for its involvement in cancer pathogenesis. However, its biological role in colorectal cancer (CRC) has remained unknown. Here, we studied the functions and mechanisms of PGM1 in CRC.

Methods: We verified *PGM-1* as a differentially expressed gene (DEG) by employing a comprehensive strategy of TCGA-COAD dataset mining and computational biology. Relative levels of PGM-1 in CRC tumors and adjoining peritumoral tissues were determined by qRT-PCR, western blotting (WB), and immunohistochemical (IHC) staining in a tissue microarray. PGM1 functions were analyzed by CCK8, EdU, colony formation, cell cycle, apoptosis, and Transwell migration and invasion assays. The influence of PGM1 was further investigated by studying tumor formation in vivo.

Results: The levels of PGM1 mRNA and protein were both reduced in CRC tissues, and the reductions were related to CRC pathology and overall survival. PGM1 knockdown stimulated both cell proliferation and colony formation, and inhibited cell cycle arrest and apoptosis, while overexpression of PGM1 produced the opposite effects in CRC cells both in vivo and in vitro. Furthermore, the effects of PGM1 were related to the PI3K/AKT pathway.

Conclusion: We verified that PGM1 suppresses CRC progression via the PI3K/AKT pathway. These results suggest the potential for targeting PGM1 in treatment of CRC.

Keywords: Phosphoglucomutase 1, Colorectal cancer, Prognosis, Proliferation, Apoptosis

Background

Colorectal cancer (CRC) results in a high number of cancer-related deaths throughout the world [1]. In the USA, 147,950 new cases of CRC were reported in 2020 and approximately 53,200 deaths are reported annually [2]. The primary therapy options mainly depend on CRC staging. The five-year survival rate for early-stage disease

exceeds 90% [1, 3]. Unfortunately, many patients already have advanced-stage disease at the time of diagnosis [4]. Therefore, there remains a need to identify reliable biomarkers and cancer-related molecular mechanisms that can assist with making decisions regarding a patient's prognosis and developing suitable therapeutic strategies.

The microenvironment of a tumor plays a critical role in its metastatic spread. Increased glycolytic activity is associated with higher microenvironmental energy demands [5, 6] and tumors are characterized by a switch from oxidative phosphorylation to glycolysis as their main energy source [7]. Biosynthesis occurring within the cell supplies the necessary components and imparts a selective advantage to neoplastic cells [8]. Phosphoglucomutase (PGM) plays a key role in glucose metabolism

[†]Zhewen Zheng and Xue Zhang have contributed equally to this work and share first authorship

*Correspondence: yfzhouwhu@163.com

¹Department of Radiation Oncology and Medical Oncology, Zhongnan Hospital of Wuhan University, 169 Donghu Road, Wuchang District, Wuhan, Hubei, People's Republic of China
Full list of author information is available at the end of the article



[9], and the enzyme has been linked to cancer growth, metastasis, and invasion [10, 11]. Phosphoglucomutase 1 (PGM1) is encoded by the *PGM1* gene; PGM1 deficiency is a recognized inherited metabolic disorder (CDG1T) that is linked to a variety of diseases and disorders, including liver disease, exercise intolerance, and dilated cardiomyopathy, reflecting the key role played by the enzyme in glucose metabolism [12–14]. PGM1 inhibits hepatocellular carcinoma cell (HCC) proliferation and growth by utilizing sufficient extracellular glucose to convert glycogen, while deletion of the *PGM1* gene inhibits glycogen synthesis and leads to glycolysis of additional glucose, thus promoting tumor cell proliferation and growth [15]. However, PGM1 showed the opposite effect in lung cancer, under glucose depletion conditions, where researchers found that an upregulation of PGM1 increased glycogen content, and thereby reduced the rates of glycogen decomposition and glycogenesis, glycogen accumulation induces cell survival and proliferation under conditions of glucose depletion, decrease in PGM1 reduces tumor cell proliferation under prolonged glucose depletion [16]. Thus, PGM1 can play a tumor-promoting or anti-tumor-promoting role in an environmentally-dependent manner.

Here, we investigated the role of PGM1 and its regulation in CRC. We identified a new mechanism by which PGM1 suppresses CRC progression by regulating glucose translocation via the PI3K/AKT pathway.

Materials and methods

TCGA data sets

Differentially expressed genes were investigated using TCGA COAD (colorectal adenocarcinoma) and READ (rectal adenocarcinoma) data sets. The Ballgown R package in Bioconductor was used to analyze differential expression in RNA-seq data. Gene expression was compared between cancer and adjoining non-cancerous tissues. P-values and differences between the q-value and fold-change were calculated using the following criteria for differential expression: $P < 0.01$, $q < 0.05$, and fold-change > 2 . GEPIA (gepia.cancer-pku.cn) was used for normalization and log₂-scaling.

Collection of clinical samples

The study protocol was approved by the Institutional Review Board of Wuhan University Zhongnan Hospital. Written informed consent was obtained from all patients prior to sample collection.

Samples (tumor and adjoining normal tissue) were collected from 76 patients with primary CRC who were admitted to Wuhan University Zhongnan Hospital between July 2019 and October 2020. The samples were

Table 1 Associations of PGM1 expression with clinicopathological factors in CRC patients

Variable	Number	PGM1 expression		P-value
		High	Low	
		(N = 38)	(N = 38)	
Age(year)				
< 65	59 (77.6%)	31 (81.6%)	28 (73.7%)	0.582
≥ 65	17 (22.4%)	7 (18.4%)	10 (26.3%)	
Gender				
Female	32 (42.1%)	12 (31.6%)	20 (52.6%)	0.104
Male	44 (57.9%)	26 (68.4%)	18 (47.4%)	
Tumor size (cm)				
< 5	41 (53.9%)	26 (68.4%)	15 (39.5%)	0.021
≥ 5	35 (46.1%)	12 (31.6%)	23 (60.5%)	
Differentiation				
Moderate	19 (25.0%)	9 (23.7%)	10 (26.3%)	0.447
Poor	34 (44.7%)	15 (39.5%)	19 (50.0%)	
Well	23 (30.3%)	14 (36.8%)	9 (23.7%)	
Lymphatic node metastasis				
Negative	42 (55.3%)	28 (73.7%)	14 (36.8%)	0.003
Positive	34 (44.7%)	10 (26.3%)	24 (63.2%)	
TNM stage				
I + II	34 (44.7%)	25 (65.8%)	9 (23.7%)	< 0.001
III + IV	42 (55.3%)	13 (34.2%)	29 (76.3%)	
Distant metastasis				
No	44 (57.9%)	27 (71.1%)	17 (44.7%)	0.037
Yes	32 (42.1%)	11 (28.9%)	21 (55.3%)	
1 years of survival				0.003
Live	62 (81.6%)	36 (94.7%)	26 (68.4%)	
Dead	14 (18.4%)	2 (5.3%)	12 (31.6%)	
5 years of survival				< 0.001
Live	29 (38.2%)	23 (60.5%)	6 (15.8%)	
Dead	47 (61.8%)	15 (39.5%)	32 (84.2%)	

kept frozen at -80°C until use. Patient clinical information is provided in Table 1.

Immunohistochemistry and scoring

Immunohistochemical analysis (IHC) was performed using a CRC tissue microarray (TMA) slide (Cat: HCo-IA180Su10; Shanghai Outdo Biotech Co., Ltd., China). The TMA included CRC tissue specimens obtained from 100 surgically resected patients during the time period of April to November 2008. The patients were followed up until July 2015 (range, 6.7–7.2 years), had a mean age of 66.83 years (range 45–91 years), and included 58 men and 41 women. Table 1 shows the clinical data for these patients. Tissue sections (4 μm thick) were cut and deparaffinized. The sections were then microwaved for 5 min in citric acid (pH 6.0), incubated

with an anti-PGM1 antibody (#15161-1-AP; Proteintech, China; 1:200), overnight at 4 °C, and then incubated with a secondary antibody. Images of the tissues were examined by two blinded pathologists and scored by multiplying the staining intensity (grades 0, 1, and 2 indicated negative; grade 3, weakly positive; grade 4, moderately positive; grade 5, strongly positive) by the positive rate score (score 0 = 0%, 1 = 0–5%, 2 = 6–25%, 3 = 26–50%, 4 = 51–75%, and 5 = 76–100%).

Cell culture

Human CRC lines HT-29, LoVo, COLO205, SW620, and HCT116, together with the normal human colorectal cell line HCoEpic, were provided by the Institute of Biochemistry and Cell Biology of the Chinese Academy of Sciences (Shanghai, China). The cells were cultured in DMEM (Gibco, Waltham, MA, USA) supplemented with 10% fetal bovine serum (FBS; Gibco) at 37 °C in a humidified chamber containing 5% CO₂.

Western blotting

Western blotting was utilized to analyze PGM1 expression in tumor tissues and cultured cells. The cells and tissues were lysed in RIPA buffer (Beyotime, Beijing, China) containing proteolytic inhibitors (Genebase, Shanghai, China), and protein concentrations were measured with a Pierce BCA Protein Assay kit (Thermo Scientific, Waltham, MA, USA). Protein extracts (30 µg) were separated on 10–12% SDS-PAGE gels, and the separated protein bands were transferred onto polyvinylidene fluoride (PVDF) membranes (Millipore, Bedford, MA, USA). The blots were probed with primary antibodies including PGM1 (Abcam, Cambridge, UK; #232959; 1:1000 dilution), PI3K (Abcam; #ab32089; 1:10,000), p-PI3K (Abcam; #ab278545; 1:10,000), AKT (Abcam; #ab8805; 1:10,000), p-AKT (Abcam; #ab38449; 1:10,000), Bcl-2 (Abcam; #ab182858; 1:10,000), Bax (Abcam; #ab32503; 1:10,000), p21 (Abcam; #ab109199; 1:10,000), Cyclin D1 (Abcam; #ab40754; 1:10,000), and GAPDH (CST, Danvers, MA, USA; #3686; 1:1000) overnight at 4 °C. Next, secondary antibodies were added at room temperature, 1 h, and immunostaining was detected with an ECL Western blotting Detection System (Amersham, Piscataway, NJ, USA). The loading control was GAPDH, and each blot was analyzed in triplicate. ImageJ software was used for a quantitative analysis of staining.

RT-PCR

The total RNA was extracted cells and tissues using TRIzol Reagent (Invitrogen, Waltham, MA, USA), and cDNA was obtained using a Bestar™ qPCR RT kit (DBI Bioscience, #2220, Germany). The PGM1 primers were

5'-AGCATTCCTGATTTCCAGCAG-3' (forward) and 5'-GCCAGTTGGGGTCTCA TACAAA-3' (reverse). The GAPDH primers were 5'-TGTTCGTCATGGGTG TGAAC-3' (forward) and 5'-ATGGCATGGACTGTGGT CAT-3' (reverse). PGM1 expression was measured by the RT-PCR that was performed using Bestar™ qPCR MasterMix (DBI Bioscience, #2043, Germany). The control gene was *GAPDH*, and relative levels of gene expression were calculated by the 2^{-ΔΔCt} method [17].

Immunofluorescence (IF)

Immunofluorescence staining of cells was performed as previously described [18]. In brief, cells were fixed in 4% paraformaldehyde for 15 min and then permeabilized with 0.1% Triton X-100 for 10 min at 4 °C. Next, the cells were incubated overnight with primary antibodies, followed by incubation with secondary antibodies (60 min, room temperature). DAPI was used for staining nuclei (5 min), and the sealed coverslips were evaluated with a laser scanning confocal microscope (Zeiss, Germany).

Immunohistochemistry (IHC), Ki 67, and H&E staining

For IHC, tissue sections were deparaffinized and endogenous peroxidase was inactivated. The sections were then blocked and incubated with anti-PGM1 (Proteintech; #15161-1-AP; 1:200) or anti-Ki67 (Bbcam; #ab15580; 1:400) primary antibodies and secondary antibodies (Abcam; #ab205718; 1:4000). For H&E staining, sections of mouse xenograft tumors were deparaffinized and then rehydrated and stained with H&E (Sigma-Aldrich, St. Louis, MO, USA) prior to dehydration and sealing. The sections were assessed and photographed under a phase contrast microscope (Leica, Cat. #DMI 1).

Transfection and plasmid construction

Cells (SW620 and HT-29) were transfected with plasmids or shRNA by using Lipofectamine 2000, according to the manufacturer's instructions. The sense sequences of PGM1 short hairpin (sh)RNA-shPGM1 were: shRNA1, 5'-GGTCCTGCTCCAGA AG CAATA-3'; shRNA2, 5'-GGGATCATCACTGGTGGTTGG-3'; shRNA3, 5'-GCAGATGGCA GCTGCCAATGG-3'. The sh-negative control (NC)-shCTRL was 5'-CAGTTGAC GAG CAGTGC ATTT-3'. The PGM1 overexpression plasmid (pcDNA4.0-PGM1) and empty plasmid (pcDNA4.0) were obtained from Synbio Technologies Co., Ltd. (Suzhou, China). To construct stable PGM1 knockdown and overexpression cell lines, HT-29 and SW620 cells were treated with lentiviral control-shRNA (shCTRL), lentiviral-PGM1-shRNA-1 (shPGM1), lentiviral- pcDNA4.0-PGM1, lentiviral- pcDNA4.0, and then selected using puromycin (5 µg/mL, Sigma).

Measurements of cell proliferation and colony formation

The CCK-8 assay (Dojindo Laboratories, Kumamoto, Japan) was used for evaluating cell proliferation. Triplicate samples of cells (2×10^3) were added to 96-well plates and the absorbance of each well at 450 nm was determined each day for three consecutive days. For measurements of colony formation, triplicate samples of treated cells (1.5×10^3) were cultured for 14 days; after which, they were washed twice with PBS, fixed in methanol for 10 min, and stained with 0.1% crystal violet for 10 min.

EDU proliferation assay

Cell proliferation was measured with an EdU kit (Ribobio, Guangzhou, China). The cells (10×10^5 per well) were inoculated into confocal plates in 50 μ M EDU buffer and then incubated at 37 °C for 2 h before fixation (4% formaldehyde, 30 min) and permeabilization (0.1% Triton X-100, 20 min). Next, EdU solution was added, the nuclei were stained with Hoechst staining solution, and the cells were evaluated under a fluorescence microscope.

Measurement of apoptosis

Transfected cells (HT-29 and SW620 cells, pcDNA4.0 vector, pcDNA4.0-PGM1 vector, NC-shRNA, or PGM1-shRNA) were harvested when they reached 90% confluence. The cells were then stained for 10–15 min in the dark at room temperature with 10 μ L of Annexin V-APC/7 solution contained in an AAD apoptosis kit (Lianke Biotech co., LTD., Hangzhou, China). Staining results were evaluated by flow cytometry (FACSCalibur, BD Biosciences, Franklin Lakes, NJ, USA).

TUNEL assay

The cells were washed twice with PBS, fixed in 4% paraformaldehyde and stained; after which, they were visualized using a one-step TUNEL kit (C1089, Beyotime Institute) as previously described [19]. Fluorescence density was analyzed using Image Pro plus 6.0 software. Sections of CRC tumors were dewaxed, incubated with proteinase K (DNase-free, 20 μ g/mL; 30 min, 37 °C), washed again, and then incubated with 50 μ L of TUNEL reagents (60 min, 37 °C, in the dark). After re-washing in PBS, the sections were evaluated under a confocal fluorescence microscope (Zeiss LSM710, Germany). Apoptotic cells were assessed in 10 randomly selected fields from six sections using Image J software.

Transwell assays

A 24-well Transwell chamber (8- μ m pore size, Corning, NY, USA) was used with or without Matrigel. Transfected

cells (5×10^4 in 300 μ L of serum-free medium) were inoculated in the upper chamber. Medium containing 10% FBS (700 μ L) was added to the lower chamber, and incubated for 24 h at 37 °C. Cells in the lower chamber were fixed with 4% paraformaldehyde and then stained with 0.5% crystal violet. Finally, five fields of each insert were randomly selected for evaluation by light microscopy (magnification, $\times 200$).

Cell cycle analysis

A cell cycle analysis was performed to determine whether PGM1 was involved in its regulation. Briefly, cells were transfected with pcDNA4.0 vector, pcDNA4.0-PGM1 vector, NC-shRNA, or PGM1-shRNA. After harvesting, triplicate samples of cells were fixed (70% ethanol, overnight, 4 °C), stained (PI, 100 μ g/mL RNAase), and assessed by flow cytometry.

Lactate measurements

Cells (2×10^5) were cultured in 12-well plates with a medium change after 10 h. After further incubation for 20 h, lactate was assayed with a Lactate Assay Kit (BioVision, Milpitas, CA, USA). Cellular glycogen levels were measured using a Glycogen Assay Kit (BioVision). Absorbances at 450 nm were read with a microplate reader and lactate concentrations (expressed as mean values \pm SD for three independent samples) were calculated from a standard curve.

ATP measurements

ATP levels were assessed by using an ATP Colorimetric/Fluorometric Assay kit (BioVision) according to the manufacturer's protocol. The levels of phosphorylated glycerol were quantitated by measuring absorbance at 570 nm.

Xenograft mice

Athymic BALB/c nude mice (4-weeks old, male) were purchased from the SLAC Laboratory Animal Co. (Shanghai, China). All study protocols were approved by the Institutional Animal Care and Use Committee of Wuhan University Zhongnan Hospital. The mice were housed in a pathogen-free location and randomly assigned to five groups (n=5 mice per group). SW620 cells (3×10^7 , either wild-type or transfected with pcDNA4.0 vector, pcDNA4.0-PGM1 vector, NC-shRNA, or PGM1-shRNA) were injected into the left flank.

Tumor volumes (calculated from caliper measurements with the formula $V = \text{length} \times \text{width}^2 \times 0.5$) were determined every third day for 4 weeks. The mice were then sacrificed and the tumors were fixed (4% paraformaldehyde, 24 h) and stained (H&E). Tumor tissues were also immunostained for PGM1 and ki67 using the following antibodies: PGM1 (Abcam; #51248; 1:500) and Ki67 (CST; #9449; 1:400). Images were recorded under a brightfield microscope (Olympus, Tokyo, Japan).

Statistical analysis

GraphPad Prism 7.0 software (GraphPad, San Diego, CA, USA) was used for data analysis. Data are presented as a mean value \pm standard deviation (SD). The t-test was used for assessing differences between two groups and one-way analysis of variance (ANOVA) was used for multiple groups. The chi-square test was used for determining the relationship between PGM1 and CRC clinical features. The cut-off value used for patient division into high and low expression groups was the median PGM1 expression value among all samples. Survival curves were evaluated by the Kaplan–Meier method and differences were measured by the log-rank test. The Cox proportional hazards model was utilized to determine independent prognostic factors. A P-value < 0.05 was considered to be statistically significant.

Results

Identification of PGM1 via TCGA datasets

We initially identified DEGs using the TCGA-CRC datasets. We found that among 5463 DEGs, 2524 (12.7%) were upregulated in normal tissues, and 2939 (14.8%) were downregulated in tumor tissues (Fig. 1A). A heat map (Fig. 1B) shows the top 54 genes that changed the most; in other words, the up- or downregulated genes that were selected for further analysis. GEPIA is an online resource that allows for visualization of TCGA and GTEx data [20]. As shown in Fig. 1C, a high level of PGM1 expression was observed in 41 normal tissues when compared to 471 colorectal tumor tissues ($P < 0.0001$).

DAVID was used to determine DEG characteristics. A GO analysis showed that DEG biological processes (BP)

were significantly enriched in “cellular metal ion homeostasis”, “muscle system process”, and “divalent inorganic cation homeostasis”. DEG cell components (CC) were largely enriched in “extracellular matrix” and “collagen-containing extracellular matrix”, while a molecular function (MF) analysis showed enrichment in “cation transmembrane activity” and “receptor regulator activity” (Fig. 1D). A KEGG pathway determination showed DEG enrichment in “neuroactive ligand-receptor interaction”, “calcium signaling pathway”, and “cytokine-cytokine receptor interaction” (Fig. 1E). Cytoscape was used for drawing a DEG PPI network and identifying significant modules (Fig. 1F).

Furthermore, follow-up data for the enrolled patients were collected for survival analysis. A Kaplan–Meier curve revealed a better overall survival rate among CRC patients with a high-level of PGM1 (Fig. 1G). ROC curves illustrated the diagnostic potential of PGM1 in CRC, with a relatively high sensitivity ($\text{AUC} = 0.635$, Fig. 1H). The aforementioned data suggested that PGM1 could be a prognostic marker for CRC.

Decreased PGM1 expression in CRC was linked to a poor prognosis

To determine the value of the PGM1 level as a CRC biomarker, we used the PCR to measure PGM1 mRNA levels in 76 pairs of tumor and matched adjoining normal tissue. It was observed that PGM1 mRNA levels in the CRC tissues were reduced when compared to the levels in non-CRC tissues ($P < 0.001$; Fig. 2A); furthermore, this difference was also revealed by WB assays (Fig. 2B, C). As verification, IHC staining was used to evaluate PGM1 protein levels in 100 CRC tissues on microarray chips (Fig. 2D), and the integrated optical density (IOD) for PGM1 expression in 100 tumor and normal samples was analyzed using GraphPad Prism software. As shown in Fig. 2E, PGM1 expression was lower in the tumor tissues ($P < 0.001$). Moreover, the high-PGM1 patient group had a better overall survival rate ($P < 0.0001$; Additional file 1: Fig. S1) than the low-PGM1 group. These results indicated that PGM1 expression was reduced in CRC tumors and PGM1 expression could affect the survival prognosis of CRC patients.

(See figure on next page.)

Fig. 1 Identification of PGM1 via TCGA datasets. **A** Volcano plot showing the distribution of DEGs in TCGA. Red color shows up-regulated genes in normal tissue while blue color shows down-regulated genes in tumor tissue. **B** A heat map of 54 core genes from the TCGA-COAD dataset comparing CRC tissue and adjoining normal tissue. **C** PGM1 expression in normal control and CRC patients based on samples listed in the TCGA database (matched TCGA normal and GTEx data, $P < 0.001$). Each dot represents one sample; **D** GO network showing relationships between DEGs and predicted functions. Vertical axis, GO category; horizontal axis, P-values. A lower P-value indicates a greater predicted involvement of the DEG in CRC+. **E** KEGG network showing connections between pathways and DEGs. Vertical axis, pathway classification; horizontal axis, P-value. A lower P-value indicates greater numbers of pathways involving DEGs. **F** PPI (protein–protein interaction) network of DEGs as drawn by Cytoscape. **G** Kaplan–Meier analysis showing the association between PGM1 expression and overall survival among CRC patients. **H** AUC curves with respect to PGM1 gene expression in the TCGA cohort. PGM, phosphoglucomutase; CRC, colorectal cancer; TCGA, The Cancer Genome Atlas; AUC, area under the curve

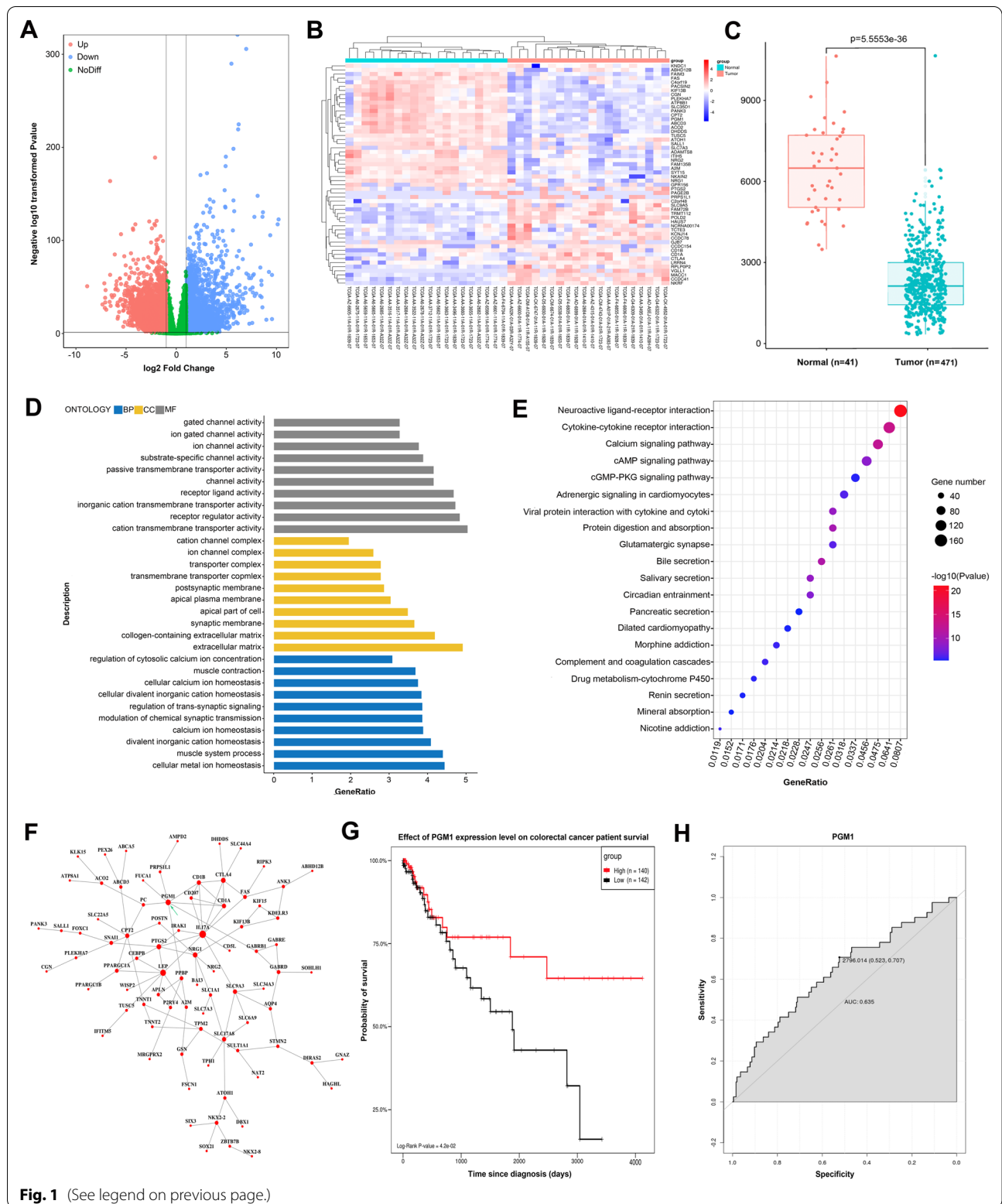
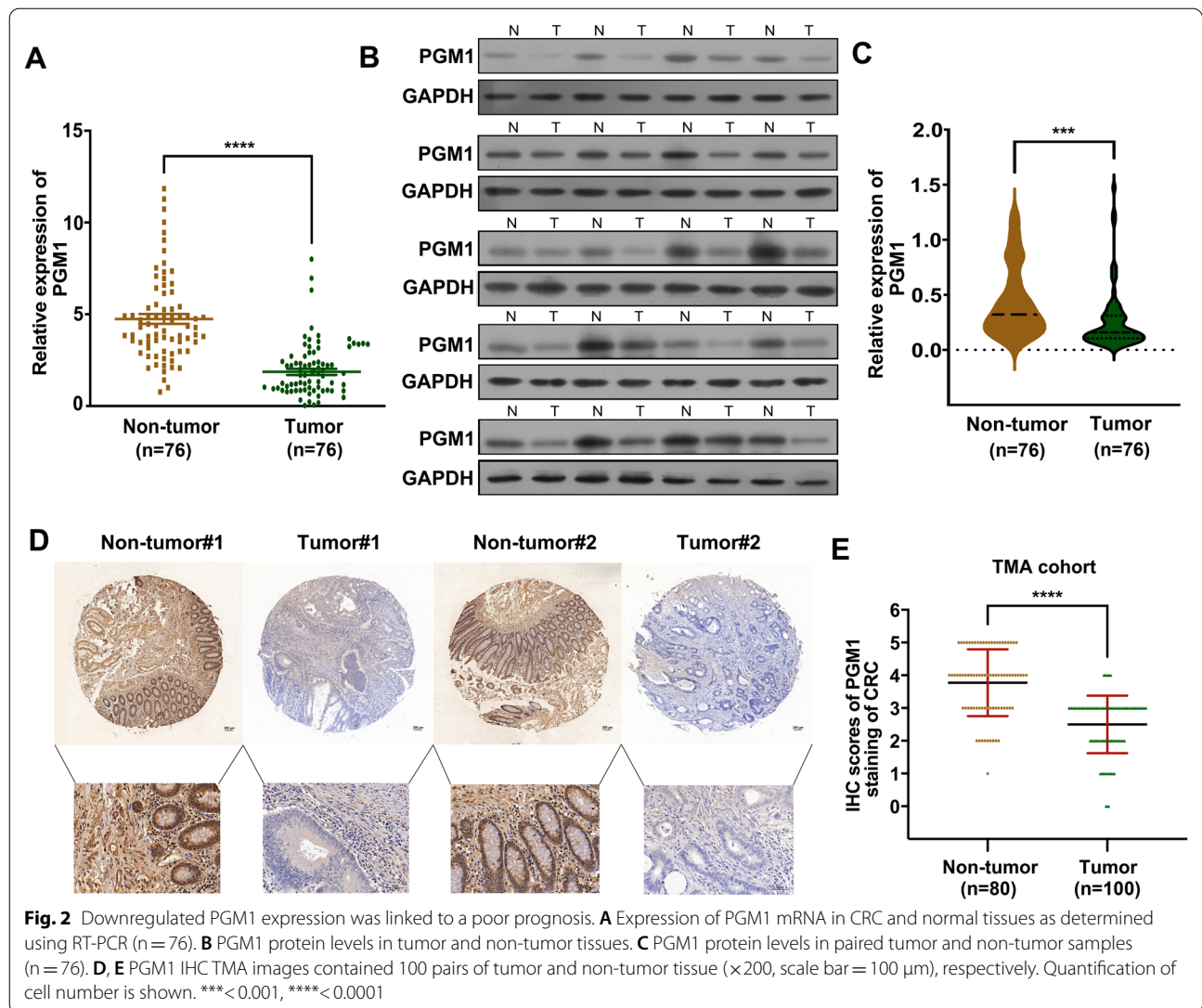


Fig. 1 (See legend on previous page.)



In order to assess the link between PGM1 levels and clinical characteristics, we collected tumor tissues and demographic data from 76 CRC patients. The median value of PGM1 expression among those tissues was 1.34. On that basis, the 76 samples were divided into high (index > 1.34, n = 38) and low (index ≤ 1.34, n = 38) PGM1 expression groups according to median value. Further analyses were conducted in different subgroups. Table 1 shows a significant difference between low- or high-PGM1 expression and “tumor size” (P = 0.0214), “lymph node metastasis” (P = 0.0027), “clinical stage” (P < 0.0010), and “distant metastasis” (P = 0.0365). However, there was no significant difference between PGM1 expression and “age”, “sex”, or “degree of tumor differentiation”. Furthermore, a multivariate analysis indicated that “lymphatic node metastasis”, “TNM stage”, and “distant metastasis”

were independent risk factors for a poor outcome in CRC patients (Table 2). Consistent with results shown in Fig. 1H, a Kaplan–Meier analysis indicated a link between lower PGM1 expression and a poorer overall survival (OS) rate. Taken together, these results indicate that PGM1 expression levels are reduced in CRC

Table 2 Multivariate analysis of the correlation between PGM1 expression and clinicopathologic parameters

Parameters	EXP (B)	P-value	OR	95% CI
Tumor size (cm): ≥ 5	− 1.114	0.063	0.328	0.101–1.063
Lymphatic node metastasis: positive	− 1.605	0.006	0.201	0.064–0.635
TNM stage: III + IV	− 1.391	0.018	0.249	0.079–0.784
Distant metastasis: yes	− 1.215	0.037	0.297	0.095–0.928

patients, and those reductions are linked to a poor prognosis.

PGM1-overexpressing and PGM1-knockdown CRC cell lines were successfully constructed

To further investigate the role of PGM1 and identify the best cell lines for overexpressing or silencing PGM1, PGM1 expression was examined in five CRC cell lines, as well as in HCoEpiC cells. Both RT-PCR and western blotting results showed that PGM1 was

most highly expressed in HT-29 cells ($P < 0.001$), and its lowest expression was in SW620 cells ($P < 0.0001$; Fig. 3A). Treatment with shRNA-1 was the most effective method of silencing *PGM1* when compared to the negative control group (shCTRL, $P < 0.001$) (Fig. 3B). Thus, the HT-29 and the SW620 cell lines were selected for silencing PGM1 expression by use of shRNA-1. In addition, we also established CRC cells (SW620 and HT-29) with lentivirus-mediated PGM1 overexpression, which was verified by both qRT-PCR and western

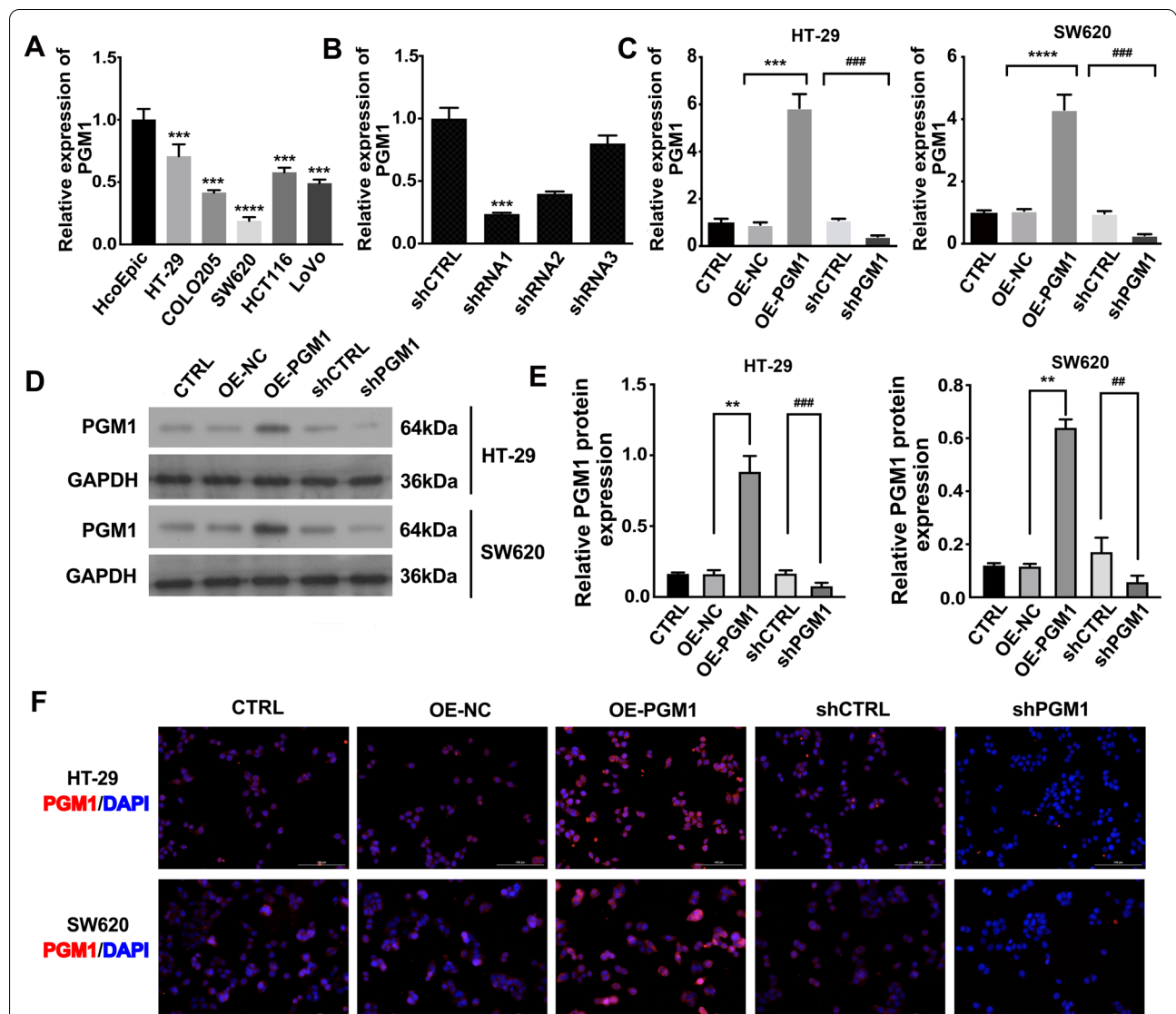
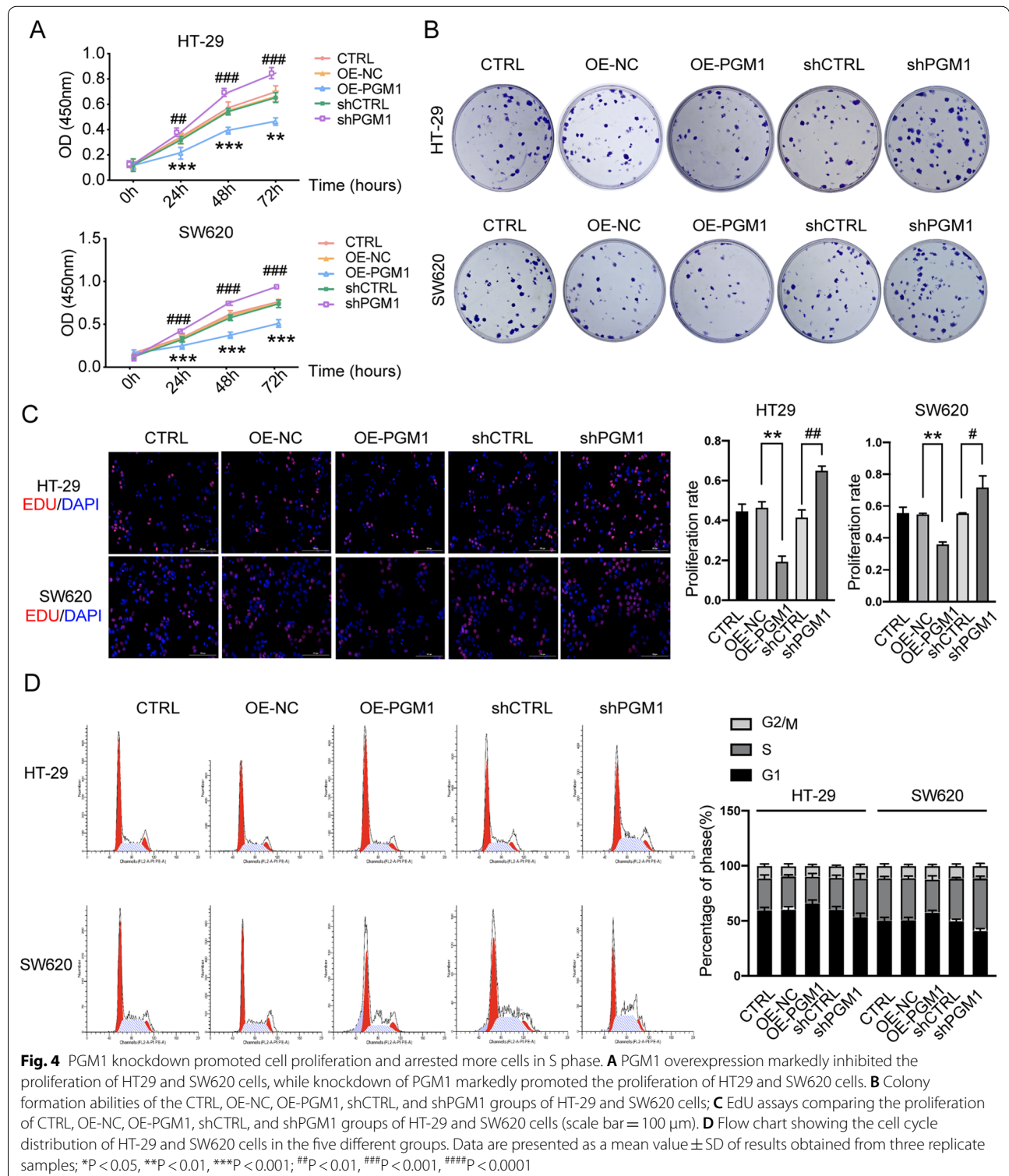


Fig. 3 Successful construction of PGM1-overexpression and knockdown cell lines. **A** PGM1 expression in CRC cells as measured by RT-PCR. **B** PGM1 mRNA in control cells and in cells transfected with PGM1 shRNA. *** $P < 0.01$ vs. shCTRL. **C** PGM1 mRNA expression in cells transfected with pcDNA4.0 vector, pcDNA4.0-PGM1 vector, NC-shRNA, or PGM1-shRNA was determined by RT-qPCR. **D, E** PGM1 protein expression in the following five groups of transfected cells: CTRL, OE-NC, OE-PGM1, shCTRL, and shPGM1. **F** Images of cells transfected with the aforementioned vectors or shRNAs after being stained for PGM1 expression (red); nuclei are stained blue (DAPI). IOD, integrated optical density; CTRL, negative control; OE, over expression. Data are presented as a mean value \pm SD of results obtained from three replicate samples; ** $P < 0.01$, *** $P < 0.001$, **** $P < 0.001$; ## $P < 0.01$, ### $P < 0.001$

blotting (Fig. 3C–E). Moreover, immunofluorescence also confirmed the above experimental results (Fig. 3F). These results all demonstrated a significant suppression

of PGM1 mRNA and protein production in sh-PRC1-transfected cells and their over-production in the pcDNA4.0-PGM1 vector transfected cell lines.



Knockdown of PGM1 promoted the proliferation and arrest of more cells in S phase

CCK8, colony-forming, and Edu assays were utilized to investigate the effects of PGM1 on cell proliferation. There was significant inhibition of proliferation in the PGM1 overexpression group when compared to the negative control group (OE-NC) ($P < 0.001$) (Fig. 4A). Similarly, PGM1-knockdown cells proliferated more rapidly than cells in the shCTRL group ($P < 0.001$). There were fewer colony numbers among cells transfected with the PGM1 overexpression vector (pcDNA4.0-PGM1) ($P < 0.01$) (Fig. 4B), while the opposite phenomenon was seen in the shPGM1 group (shPGM1) when compared with the shCTRL group. Moreover, EDU assays also showed reduced cell proliferation in the PGM1 overexpression group, but enhanced proliferation in the PGM1 knockdown group (Fig. 4C).

The cell cycle distribution of cells in the different groups (CTRL, OE-NC, OE-PGM1, shCTRL, and shPGM1) was examined by PI staining. PGM1 silencing resulted in a significant accumulation of S-phase cells and a reduction in G0/G1-phase cells, while the percentages of G2/M-phase cells remained largely unchanged (Fig. 4D). PGM1 overexpression led to reduced percentages of S-phase cells and increased percentages of G1-phase cells. These results suggest that PGM1 suppresses tumor growth by regulating cell proliferation and enhancing the numbers of S-phase cells.

PGM1 promotes apoptosis in CRC cells

Apoptosis is an important factor in CRC pathology. To investigate whether PGM1 acts as a cancer suppressor by modulating apoptosis, we evaluated apoptosis via the FCM and TUNEL assays. Flow cytometry results showed that in contrast to the shCTRL group, there was a reduced rate of apoptosis among the shPGM1 transfected cells, and an increased rate of apoptosis among the PGM1 overexpression cells (Fig. 5A, B). Moreover, TUNEL assays showed that apoptosis was enhanced in the OE-PGM1 group when compared with the OE-NC group (Fig. 5C, D). On the contrary, PGM1 knockdown greatly decreased HT-29 and SW620 cell apoptosis. These data showed that PGM1 promoted the apoptosis of CRC cells in vitro.

PGM1 inhibited cell migration and invasion

Transwell assays were performed to evaluate the invasive and migratory capacities of colorectal cancer cells influenced by PGM1. Consistent with our previous hypothesis, we found that PGM1 up-regulation markedly reduced cell migration (Fig. 6A, B) and invasion (Fig. 6C, D). On the contrary, PGM1 silencing markedly reduced

both of those parameters (Fig. 6A–D). These findings further confirmed that PGM1 acts as a tumor-suppressing factor in CRC.

PGM1 suppressed CRC progression via the PI3K/AKT pathway

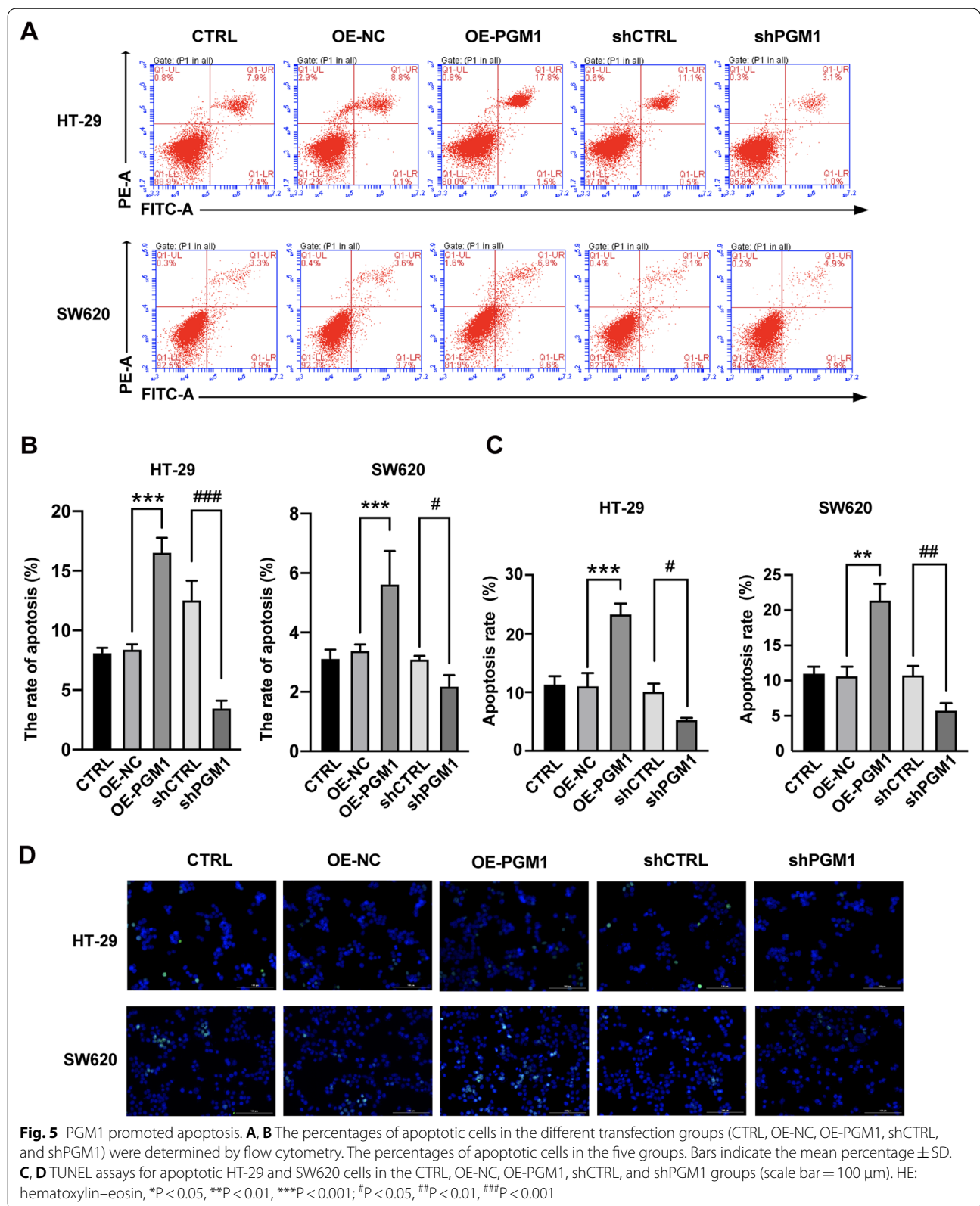
Because we hypothesized that PGM1 might inhibit CRC cell proliferation by downregulating PI3K/AKT signaling, we assessed the levels of p-PI3K and p-AKT in CRC cells. The diminished p-PI3K and p-AKT protein levels induced by PGM1 overexpression substantially increased after the CRC cells were transfected with shPGM1 (Fig. 7A, B). Therefore, we conclude that to some extent, PGM1 inhibits CRC progression by activating the PI3K/AKT pathway.

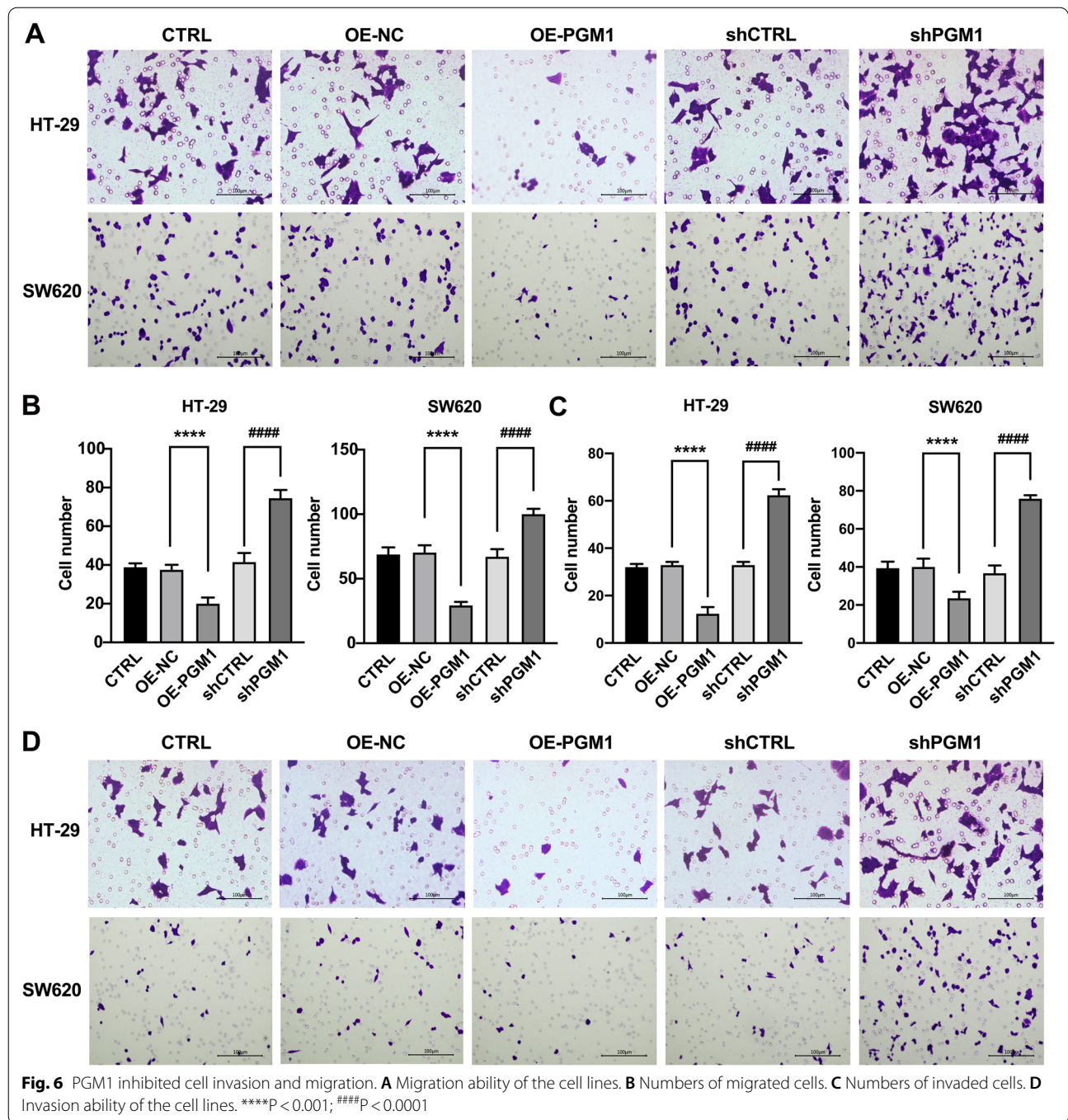
We also assessed apoptosis-related proteins. We observed that PGM1 positively regulated Bax and negatively regulated Bcl-2 ($P < 0.05$) (Fig. 7A, B). Thus, it appears that PGM1 exerts a tumor suppressive effect by regulating both apoptosis and the S phase of cells.

In terms of cell cycle-related proteins, we found a down-regulation of G1 inhibitors (p21) ($P < 0.0001$) and an up-regulation of regulatory proteins (Cyclin D1) in shPGM1-transfected cells ($P < 0.0001$, Fig. 7A, B). In contrast, p21 levels were increased ($P < 0.0001$) and Cyclin D1 levels were decreased in response to PGM1 overexpression.

Knockdown of PGM1 accelerated tumor growth via the PI3K/AKT pathway

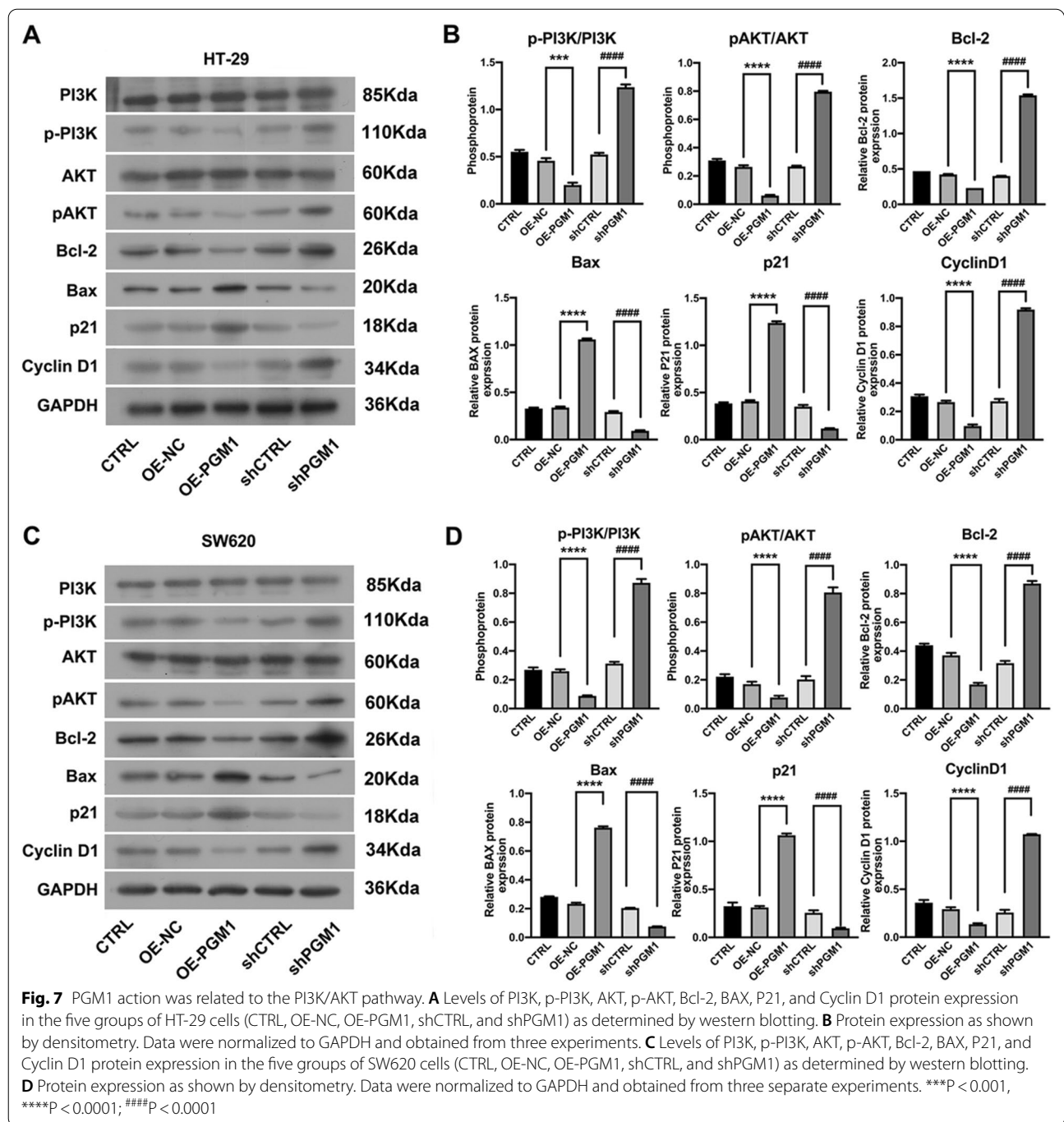
A mouse tumor model was used to investigate the action of PGM1 in vivo. SW620 cells transfected with pcDNA4.0 vector, pcDNA4.0-PGM1 vector, NC-shRNA, or PGM1-shRNA were injected into the mice; after which, PGM1 mRNA expression in five groups of tumors formed by the different treated cells was determined by RT-PCR (Fig. 8D). Consistent with the previous results of cell experiments, it was observed that tumors in the knockdown group (shPGM1) were markedly larger than those in the shCTRL group ($P < 0.0001$), and tumors in the PGM1 overexpression group (OE-PGM1) were smaller than those in the control group (OE-NC, $P < 0.001$) (Fig. 8A–C). H&E staining was used to visualize the morphological changes in each group (Fig. 8G). An immunohistochemical analysis of the tumor tissues indicated reduced expression of the differentiation marker Ki67 ($P < 0.05$, Fig. 8E and G). Moreover, TUNEL assays showed that PGM1 overexpression (OE-PGM1) led to more apoptosis than in the control group (OE-NC), while apoptosis was reduced in the PGM1 knockdown group (shPGM1) when compared with the shCTRL group (Fig. 8F and G). Thus, PGM1 inhibition led to a suppression of CRC growth and enhanced





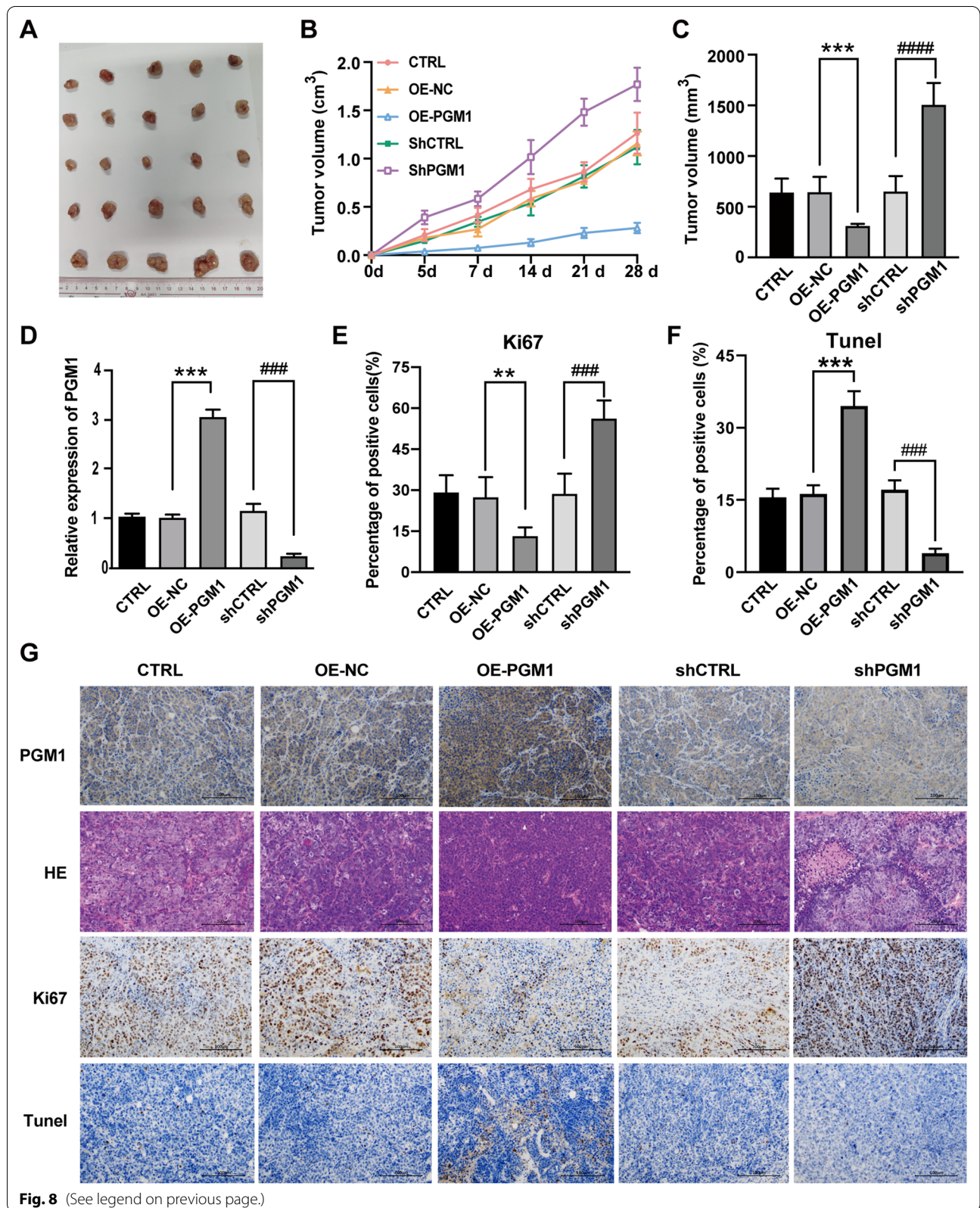
cell differentiation. Furthermore, we used a PI3K/AKT inhibitor (LY294002) to block activation of the PI3K/AKT pathway. Cell proliferation increased to its highest level in the shPGM1 group, but this phenomenon was abolished by blocking the PI3K/AKT pathway in the shPGM1 + LY group as detected by CCK8 colony formation assays (Additional file 2: Fig. S2A, B). Western blotting was

used to examine changes in p-PI3K and p-AKT expression (Additional file 2: Fig. S2C). Similarly, the increased cell migration and invasion capabilities observed in the shPGM1 group were diminished by LY294002 (Additional file 2: Fig. S2D–G). These results further confirmed that PGM1 inhibits CRC progression by activating the PI3K/AKT pathway.



(See figure on next page.)

Fig. 8 Downregulation of PGM1 accelerated tumor growth in vivo. **A** Tumors formed at 6 weeks post-injection ($n = 5$ /group). Tumors in the CTRL, OE-NC, OE-PGM1, shCTRL and shPGM1 groups were removed upon completion of the study. **B** Tumor growth in the 5 groups was assessed by measurements of tumor volume over time (mean \pm SD; $n = 25$). ** $P < 0.01$. Mice were anesthetized and sacrificed at experimental endpoints. The tumors were subsequently dissected. **C** Tumor volume was monitored in the five aforementioned groups at the endpoints in each experiment. **D** PGM1 mRNA expression in tumors from the CTRL, OE-NC, OE-PGM1, shCTRL, and shPGM1 groups; $n = 5$. **E** Representative images of PGM1 IHC, H&E, Ki67, and TUNEL staining in the CTRL, OE-NC, OE-PGM1, shCTRL, and shPGM1 groups, respectively. ($\times 200$, scale bars = 100 μ m). ** $P < 0.01$, **** $P < 0.001$, ### $P < 0.001$, #### $P < 0.0001$



PGM1 regulated glycolysis to affect cancer metabolism

Aberrant metabolism is a major hallmark of cancer. PGM1 may assist in rebalancing glycogen synthesis and glycolysis by reversibly facilitating phosphate transfer during glucose metabolism. Based on that hypothesis, we investigated whether PGM1 played a role in glucose metabolism. It was found that PGM1 overexpression inhibited both lactate and ATP production in HT-29 cells, while PGM1 knockdown produced the opposite effects. Furthermore, these results

were also confirmed in SW620 cells (Fig. 9A, B). These results indicated that PGM1 is involved in aerobic glycolysis occurring in CRC cells.

Discussion

There are five proteins in the PGM superfamily: PGM1, PGM2, PGM2L1, PGM3, and PGM5. Despite their structural similarities, the substrates and functions of these proteins differ [9, 21, 22]. For example, PGM3 is an N-acetylglucosamine triphosphatase that participates in

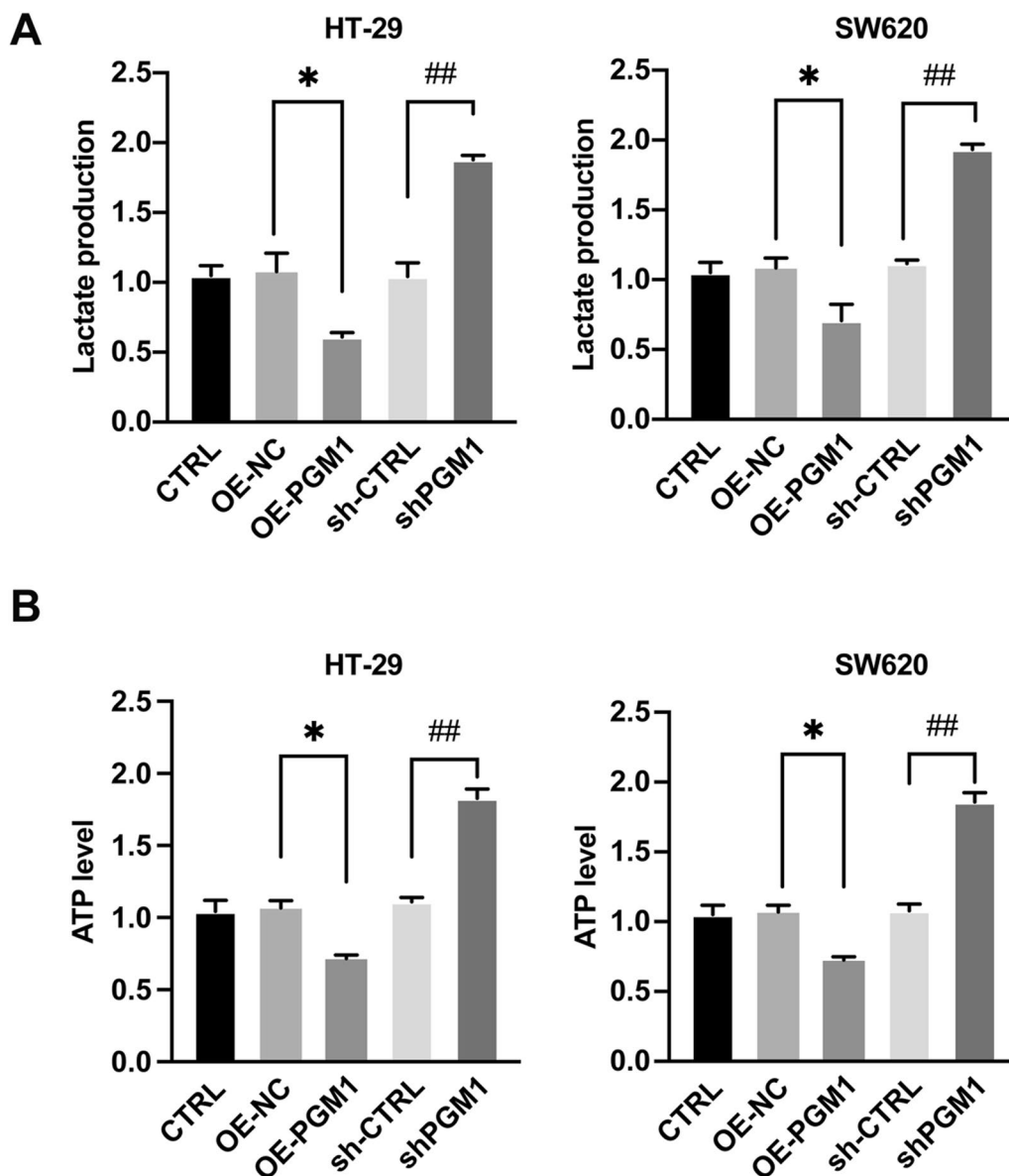


Fig. 9 PGM1 inhibited aerobic glycolysis in CRC cells. **A, B** Cells were transfected with lentivirus expressing CTRL, OE-NC, OE-PGM1, shCTRL or shPGM1. Culture media was used for determining lactate production (**A**) and ATP levels (**B**) of the cells. Data are presented as a mean value \pm SD of results obtained from three separate experiments. * $P < 0.05$, ## $P < 0.01$

alanine biosynthesis and has anti-neoplastic functions. Targeting of PGM3 inhibits the hexosamine synthetic pathway and has been found to result in growth arrest and apoptosis in breast cancer cells [23]. Furthermore, a blockade of PGM3 expression with sulforaphane was shown to promote apoptosis in prostate cancer cells [24]. PGM5 is highly expressed in muscle connections [25], and its expression level is predictive of overall survival in CRC [10]. The roles of PGM1 in glucose homeostasis and post-translational glycosylation are well characterized, and the enzyme also plays an important role in glucose trafficking by catalyzing the conversion of G1-P to G6-P. PGM1 deficiency is recognized as an inherited metabolic disorder (CDG1T) [21] that is associated with a variety of phenotypes, including exercise intolerance, dilated cardiomyopathy, and liver disease, indicating that PGM1 plays a role in glucose metabolism [26]. However, the role played by PGM1 in cancer has remained poorly understood.

Studies on the role of PGM1 in cancer are limited. Recent investigations have shown that PGM1 blocks liver cancer progression by regulating glucose trafficking [15]. Nevertheless, high levels of PGM1 have been found in lung tumors, and were shown to correlate with a poor prognosis. Li et al. [16] suggested that glucose deprivation results in increased PGM1 expression that enhances cancer progression, suggesting the possibility of targeting PGM1 in treatment of cancer. However, PGM1 does not show consistent expression patterns in different cancer types, and this might be related to the content of muscle.

Cancer metastasis involves factors related to both the tumor and its microenvironment [27]. The microenvironment is comprised of neighboring tumor cells, extracellular matrix, and interstitial tissue [28–30]. The rapid proliferation of tumors requires a significant amount of resources, and tumors are characterized by alterations in their metabolism [31] that involve a reconstruction of energy metabolism [32].

PGM1 is vital for glucose metabolism, and its absence leads to deficiencies in glycogen metabolism, that in turn, result in disease [33–35]. Specifically, *PGM1* encodes for a phosphoglucomutase associated with carbohydrate metabolism [7]. Therefore, we hypothesized that reduced levels of PGM1 might adversely affect energy metabolism, leading to a remodeling of tumor cell physiology with a shift toward the use of aerobic glycolysis. We also demonstrated that a reduction of PGM1 levels in CRC cells stimulates both cellular proliferation and tumor growth by causing the cells to shift from glycogen synthesis and divert glucose to glycolytic pathways. Our results suggest that PGM1 plays a unique, glucose-dependent

role in the suppression of CRC tumors. It was recently found that the roles played by PGM1 in glycogen and glucose metabolism are responsible for suppressing the proliferation of cervical and breast cancer cells [36], and our current results support those findings. All these results suggest that PGM1 might promote or inhibit tumor formation based on the type of tumor and its microenvironment.

PI3K/Akt signaling promotes cell proliferation and survival, and is associated with neoplastic transformation and apoptosis inhibition [37]. It is also known that an aberrant expression of proteins in the PI3K/Akt pathway is linked to the progression of various cancers [38–40]. Apart from proliferation, the PI3K/Akt pathway is also linked to cell migration and autophagy [41, 42]. Therefore, research on PGM1 and whether it targets the PI3K/AKT pathway may be significant for the management of CRC. Here, we demonstrated that the PI3K/AKT pathway is closely linked to PGM1 expression and functions to maintain cancer cell survival and proliferation. This association is important for developing new therapeutic strategies, and indicates that targeting of glycogen metabolism and (or) PGM1 expression may be useful for treating a variety of cancers that show aberrations in these pathways as well as PGM1 expression.

Taken together, these findings show that PGM1 suppresses CRC by regulating glucose translocation via the PI3K/AKT pathway, and suggest PGM1 as a potential target for detecting and treating CRC.

Conclusion

Our data showed that PGM1 suppresses CRC progression and that PGM1 levels are significantly downregulated in CRC tissues. In addition, lower levels of PGM1 were associated with a poor prognosis. Moreover, overexpression of PGM1 reduced the proliferation, invasion, and migration of CRC cells. Thus PGM1 might be a new biomarker and therapeutic target for CRC.

Abbreviations

PGM: Phosphoglucomutase; CRC: Colorectal cancer; TCGA: The Cancer Genome Atlas; DEG: Differentially expressed genes; TMA: Tissue microarray.

Supplementary Information

The online version contains supplementary material available at <https://doi.org/10.1186/s12935-022-02545-7>.

Additional file 1: Fig S1. PGM1 as a prognostic marker. High PGM1 levels were associated with better overall survival ($P = 0.0426$) in 76 samples collected by our group.

Additional file 2: Fig S2. PGM1-mediated tumor suppression was blocked by a PI3K/AKT inhibitor (LY294002) in vitro. **A** CCK8 assay comparing HT-29 and SW620 cell proliferation in the CTRL, shCTRL, shPGM, shCTRL + LY, and shPGM1 + LY groups. **B** Colony formation ability of HT-29 and SW620 cells in the different groups. **C** Levels of PI3K, p-PI3K, AKT, and p-AKT expression in cells in the 5 groups (CTRL, shCTRL, shPGM, shCTRL + LY, and shPGM1 + LY groups) as determined by western blotting. **D**, **E** Migration ability of cells in the CTRL, shCTRL, shPGM, shCTRL + LY, and shPGM1 + LY groups as detected by Transwell assays. **F**, **G** Invasion ability of cells in the CTRL, shCTRL, shPGM1, shCTRL + LY, and shPGM1 + LY groups as detected by Transwell assays. ** $P < 0.01$, *** $P < 0.001$; ## $P < 0.01$, ### $P < 0.001$. &&& $P < 0.01$, &&& $P < 0.001$.

Acknowledgements

We thank all those who participated in this study.

Authors' contributions

Conception and design: YFZ. Development of methodology: ZWZ, XZ, and JB. Data acquisition: ZWZ, XZ, JB, LL, and DL. Analysis and interpretation of data: LL and DL. Writing, review, and/or revision of the manuscript: YFZ, XZ, and ZWZ wrote the initial draft and all authors reviewed the manuscript. Study Supervision: YFZ and ZWZ. All authors read and approved the final manuscript.

Funding

This study was financially supported by the National Natural Science Foundation of China (No. 81472799), the National Natural Science Foundation of China (No. 82103553), and the Research Foundation of Beijing Friendship Hospital, Capital Medical University (No. yydqkt2020-6).

Availability of data and materials

The datasets used in this study are available from the corresponding author upon reasonable request.

Declarations

Ethics approval and consent to participate

All patient samples used for experiments were obtained with the ethical approval of Wuhan University Zhongnan Hospital.

Consent for publication

All authors of this paper have provided their signed written consent for publication in your journal.

Competing interests

All authors declare having no conflicts of interest.

Author details

¹Department of Radiation Oncology and Medical Oncology, Zhongnan Hospital of Wuhan University, 169 Donghu Road, Wuchang District, Wuhan, Hubei, People's Republic of China. ²Department of General Practice, Beijing Friendship Hospital, Capital Medical University, Beijing 100050, People's Republic of China. ³Department of Anesthesiology, Peking University Third Hospital, Beijing 100191, People's Republic of China.

Received: 29 September 2021 Accepted: 8 March 2022

Published online: 25 May 2022

References

- Brody H. Colorectal cancer. *Nature*. 2015;521:S1. <https://doi.org/10.1038/521S1a>
- Siegel RL, Miller KD, Jemal A. Cancer statistics, 2020. *CA Cancer J Clin*. 2020;70:7–30. <https://doi.org/10.3322/caac.21590>.
- Modest DP, Pant S, Sartore-Bianchi A. Treatment sequencing in metastatic colorectal cancer. *Eur J Cancer*. 2019;109:70–83. <https://doi.org/10.1016/j.ejca.2018.12.019>.
- Ladabaum U, Dominitz JA, Kahi C, Schoen RE. Strategies for colorectal cancer screening. *Gastroenterology*. 2020;158:418–432. <https://doi.org/10.1053/j.gastro.2019.06.043>.
- Abbaszadeh Z, Çeşmeli S, Avcı CB. Crucial players in glycolysis: Cancer progress. *Gene*. 2020;726:144158. <https://doi.org/10.1016/j.gene.2019.144158>.
- Zhang X, Zhao H, Li Y, Xia D, Yang L, Ma Y, Li H. The role of YAP/TAZ activity in cancer metabolic reprogramming. *Mol Cancer*. 2018;17:134. <https://doi.org/10.1186/s12943-018-0882-1>.
- Ashton TM, McKenna WG, Kunz-Schughart LA, Higgins GS. Oxidative phosphorylation as an emerging target in cancer therapy. *Clin Cancer Res*. 2018;24:2482–2490. <https://doi.org/10.1158/1078-0432.CCR-17-3070>.
- Koppenol WH, Bounds PL, Dang CV. Otto Warburg's contributions to current concepts of cancer metabolism. *Nat Rev Cancer*. 2011;11:325–37. <https://doi.org/10.1007/s00109-011-0730-x>.
- Muenks AG, Stiers KM, Beamer LJ. Sequence-structure relationships, expression profiles, and disease-associated mutations in the paralogs of phosphoglucomutase 1. *PLoS One*. 2017;12:e0183563. <https://doi.org/10.1371/journal.pone.0183563>.
- Sun Y, Long H, Sun L, Sun X, Pang L, Chen J, et al. PGM5 is a promising biomarker and may predict the prognosis of colorectal cancer patients. *Cancer Cell Int*. 2019;19:253. <https://doi.org/10.1186/s12935-019-0967-y>.
- Curtis M, Kenny HA, Ashcroft B, Mukherjee A, Johnson A, Zhang Y, et al. Fibroblasts mobilize tumor cell glycogen to promote proliferation and metastasis. *Cell Metab*. 2019;29:141–155.e9. <https://doi.org/10.1016/j.cmet.2018.08.007>.
- Conte F, Morava E, Bakar NA, Wortmann SB, Poerink AJ, Grunewald S, et al. Phosphoglucomutase-1 deficiency: Early presentation, metabolic management and detection in neonatal blood spots. *Mol Genet Metab*. 2020;131:135–146. <https://doi.org/10.1016/j.ymgme.2020.08.003>.
- Beamer LJ. Enzyme dysfunction at atomic resolution: Disease-associated variants of human phosphoglucomutase-1. *Biochimie*. 2021;183:44–8. <https://doi.org/10.1016/j.biochi.2020.08.017>.
- Fernlund E, Andersson O, Ellegård R, Åstrand HK, Green H, Olsson H, et al. The congenital disorder of glycosylation in PGM1 (PGM1-CDG) can cause severe cardiomyopathy and unexpected sudden cardiac death in childhood. *Forensic Sci Int Genet*. 2019;43:102111. <https://doi.org/10.1016/j.fsigen.2019.06.012>.
- Jin GZ, Zhang Y, Cong WM, Wu X, Wang X, Wu S, et al. Phosphoglucomutase 1 inhibits hepatocellular carcinoma progression by regulating glucose trafficking. *PLoS Biol*. 2018;16:e2006483. <https://doi.org/10.1371/journal.pbio.2006483>.
- Li Y, Liang R, Sun M, Li Z, Sheng H, Wang J, et al. AMPK-dependent phosphorylation of HDAC8 triggers PGM1 expression to promote lung cancer cell survival under glucose starvation. *Cancer Lett*. 2020;478:82–92. <https://doi.org/10.1016/j.canlet.2020.03.007>.
- Livak KJ, Schmittgen TD. Analysis of relative gene expression data using real-time quantitative PCR and the 2(-Delta Delta C(T)) Method. *Methods*. 2001;25:402–8. <https://doi.org/10.1006/meth.2001.1262>.
- Im K, Mareninov S, Diaz MFP, Yong WH. An introduction to performing immunofluorescence staining. *Methods Mol Biol*. 2019;1897:299–311. https://doi.org/10.1007/978-1-4939-8935-5_26.
- Wang X-W, Tian R-M, Yang Y-Q, Lu Z-Y, Han X-D, Liu X-S, et al. Triptolide antagonizes triptolide-induced nephrocyte apoptosis via inhibiting oxidative stress in vitro and in vivo. *Biomed Pharmacother*. 2019;118:109232. <https://doi.org/10.1016/j.biopha.2019.109232>.
- Tang Z, Li C, Kang B, Gao G, Li C, Zhang Z. GEPIA: a web server for cancer and normal gene expression profiling and interactive analyses. *Nucleic Acids Res*. 2017;45:W98–W102. <https://doi.org/10.1093/nar/gkx247>.
- Altassan R, Radenkovic S, Edmondson AC, Barone R, Brasil S, Cechova A, et al. International consensus guidelines for phosphoglucomutase 1 deficiency (PGM1-CDG): Diagnosis, follow-up, and management. *J Inher Metab Dis*. 2021;44:148–163. <https://doi.org/10.1002/jimd.12286>.
- Liu JJ, Zhang GC, Kong II, Yun EJ, Zheng JQ, Kweon DH, et al. A mutation in pgm2 causing inefficient galactose metabolism in the probiotic yeast *Saccharomyces boulardii*. *Appl Environ Microbiol*. 2018;84:e02858–17. <https://doi.org/10.1128/AEM.02858-17>.
- Ricciardiello F, Votta G, Palorini R, Raccagni I, Brunelli L, Paiotta A, et al. Inhibition of the hexosamine biosynthetic pathway by targeting PGM3

- causes breast cancer growth arrest and apoptosis. *Cell Death Dis.* 2018;9:377. <https://doi.org/10.1038/s41419-018-0405-4>.
24. Lee C-H, Jeong S-J, Yun S-M, Kim J-H, Lee H-J, Ahn KS, et al. Down-regulation of phosphoglucomutase 3 mediates sulforaphane-induced cell death in LNCaP prostate cancer cells. *Proteome Sci.* 2010;8:67. <https://doi.org/10.1186/1477-5956-8-67>.
 25. Ran F, Zhang Y, Shi Y, et al. miR-1224-3p Promotes breast cancer cell proliferation and migration through pgm5-mediated aerobic glycolysis. *J Oncol.* 2021;2021:5529770. <https://doi.org/10.1155/2021/5529770>.
 26. Tian W-T, Luan X-H, Zhou H-Y, Zhang C, Huang XJ, Liu X-L, et al. Congenital disorder of glycosylation type 1T with a novel truncated homozygous mutation in PGM1 gene and literature review. *Neuromuscul Disord.* 2019;29:282–289. <https://doi.org/10.1016/j.nmd.2019.01.001>.
 27. Laplane L, Duluc D, Bikfalvi A, Larmonier N, Pradeu T. Beyond the tumour microenvironment. *Int J Cancer.* 2019;145:2611–2618. <https://doi.org/10.1002/ijc.32343>.
 28. Arneth B. Tumor microenvironment. *Medicina (Kaunas).* 2019;56:15. <https://doi.org/10.3390/medicina56010015>.
 29. McAllister SS, Weinberg RA. The tumour-induced systemic environment as a critical regulator of cancer progression and metastasis. *Nat Cell Biol.* 2014;16:717–727. <https://doi.org/10.1038/ncb3015>.
 30. Wu T, Dai Y. Tumor microenvironment and therapeutic response. *Cancer Lett.* 2017;387:61–68. <https://doi.org/10.1016/j.canlet.2016.01.043>.
 31. Ganapathy-Kanniappan S, Geschwind JF. Tumor glycolysis as a target for cancer therapy: progress and prospects. *Mol Cancer.* 2013;12:152. <https://doi.org/10.1186/1476-4598-12-152>.
 32. Hanahan D, Weinberg RA. Hallmarks of cancer: the next generation. *Cell.* 2011;144:646–674. <https://doi.org/10.1016/j.cell.2011.02.013>.
 33. Tegtmeyer LC, Rust S, van Scherpenzeel M, Ng BG, Losfeld ME, et al. Multiple phenotypes in phosphoglucomutase 1 deficiency. *N Engl J Med.* 2014;370(6):533–542. <https://doi.org/10.1056/NEJMoa1206605>.
 34. Adeva-Andany MM, Perez-Felpete N, Fernandez-Fernandez C, et al. Liver glucose metabolism in humans. *Biosci Rep.* 2016;36(6):e00416. <https://doi.org/10.1042/BSR20160385>.
 35. Beamer LJ. Mutations in hereditary phosphoglucomutase 1 deficiency map to key regions of enzyme structure and function. *J Inherit Metab Dis.* 2015;38(2):243–256. <https://doi.org/10.1007/s10545-014-9757-9>.
 36. Bae E, Kim HE, Koh E, Kim KS. Phosphoglucomutase 1 is necessary for sustained cell growth under repetitive glucose depletion. *FEBS Lett.* 2014;588(17):3074–80. <https://doi.org/10.1016/j.febslet.2014.06.034>.
 37. Chelh I, Picard B, Hocquette JF, Cassar-Malek I. Myostatin inactivation induces a similar muscle molecular signature in double-muscled cattle as in mice. *Animal.* 2011;5(2):278–86. <https://doi.org/10.1017/S175173110001862>.
 38. Marquard FE, Jücker M. PI3K/AKT/mTOR signaling as a molecular target in head and neck cancer. *Biochem Pharmacol.* 2020;172:113729. <https://doi.org/10.1016/j.bcp.2019.113729>.
 39. Alzahrani AS. PI3K/Akt/mTOR inhibitors in cancer: at the bench and bedside. *Semin Cancer Biol.* 2019;59:125–132. <https://doi.org/10.1016/j.semcancer.2019.07.009>.
 40. Sharma VR, Gupta GK, Sharma AK, Batra N, Sharma DK, Joshi A, Sharma AK. PI3K/Akt/mTOR intracellular pathway and breast cancer: factors, mechanism and regulation. *Curr Pharm Des.* 2017;23(11):1633–1638. <https://doi.org/10.2174/1381612823666161116125218>.
 41. Park JY, Kang SE, Ahn KS, Um JY, Yang WM, Yun M, et al. Inhibition of the PI3K-AKT-mTOR pathway suppresses the adipocyte-mediated proliferation and migration of breast cancer cells. *J Cancer.* 2020;11(9):2552–2559. <https://doi.org/10.7150/jca.37975>.
 42. Xu Z, Han X, Ou D, Liu T, Li Z, Jiang G, et al. Targeting PI3K/AKT/mTOR-mediated autophagy for tumor therapy. *Appl Microbiol Biotechnol.* 2020;104(2):575–587. <https://doi.org/10.1007/s00253-019-10257-8>.

Publisher's Note

Springer Nature remains neutral with regard to jurisdictional claims in published maps and institutional affiliations.

Ready to submit your research? Choose BMC and benefit from:

- fast, convenient online submission
- thorough peer review by experienced researchers in your field
- rapid publication on acceptance
- support for research data, including large and complex data types
- gold Open Access which fosters wider collaboration and increased citations
- maximum visibility for your research: over 100M website views per year

At BMC, research is always in progress.

Learn more biomedcentral.com/submissions

